15

Thermal stabilization system for a multi-element scintillation screen

© A.V. Anisyonkov,[1] S.V. Karpov,[1] A.N. Kozyrev,[1,2,3] A.A. Ruban,[1] G.V. Stavriyetski,[4] D.N. Shepelev,[4] O.A. Nikitin[4]

[1] Budker Institute of Nuclear Physics, Siberian Branch, Russian Academy of Sciences
630090 Novosibirsk, Russia
[2] Novosibirsk State University,
630090 Novosibirsk, Russia
[3] Novosibirsk State Technical University,
630073 Novosibirsk, Russia
[4] All-Russia Research Institute of Technical Physics, Russian Federal Nuclear Center,
456770 Snezhinsk, Chelyabinsk oblast, Russia
e-mail: S.V.Karpov@inp.nsk.su

Received June 18, 2024
Revised September 25, 2024
Accepted September 27, 2024

A thermal stabilization system for a multi-element scintillation screen consisting of bismuth orthogermanate BGO crystals has been developed and tested. Thermal stabilization is necessary to improve the energy resolution of the screen, since the light output of the crystals depends on temperature. The main characteristics of the system are measured, such as the time of cooling the screen to the required operating temperature, long-term stability and uniformity of temperature distribution over the screen. The effects of changes in environmental conditions or malfunction of individual elements of the thermal stabilization system on the stability and uniformity of the screen temperature is investigated. It is shown that the thermal stabilization system provides high long-term stability and temperature uniformity with an accuracy of $\pm 0.05\,^{\circ}\mathrm{C}$, which made it possible to obtain an energy resolution of the screen of 0.5%.

Keywords: detector, scintillation, bismuth orthogermanate, BGO, thermal stabilization.

DOI: 10.61011/TP.2024.11.59760.207-24

Introduction

Budker Institute of Nuclear Physics of SB RAS jointly with Russian Federal Nuclear Center; Zababakhin All-Russia Research Institute of Technical Physics created a detector based on a multi-element scintillation screen (MSS) [1,2] for recording fluxes of hard gamma quanta. This device can be used for pulsed radiography of objects with high atomic numbers and large optical thicknesses, in particular, when they are deformed during fast-flowing processes.

Hard gamma quanta are recorded in the MSS using scintillation crystals. Lutetium-yttrium orthosilicate LYSO, lutetium orthosilicate LSO and bismuth orthogermanate BGO are the most suitable scintillators for such a detector in terms of density, attenuation time and light output. These scintillators are commonly used in calorimeters [3–9] and in positron emission tomographs [10–13]. Only BGO crystals are currently produced in mass quantities in Russia. BGO crystals produced by A.V. Nikolaev Institute of Inorganic Chemistry are used to record gamma quanta in MSS [14]. This type of crystals have such advantages as high atomic number, relatively high light output, and good chemical and mechanical stability. The disadvantages include a strong dependence of the light output on temperature. The light output decreases by 1.55% when the temperature increases by 1.°C. For this reason it is necessary to ensure the temperature stabilization of the detector for obtaining a high energy resolution. Previously, a similar problem was successfully solved for the development of a calorimeter based on BGO crystals, which is part of the CMD-3 elementary particle detector used in the Budker Institute of Nuclear Physics of SB RAS at the acceleration complex VEPP-2000. The calorimeter copper ring support accommodating modules consisting of crystals with photodetectors and charge-sensitive amplifiers is cooled by water for thermal stabilization of crystals. The stability of crystal temperature $\pm 1\,^{\circ}\mathrm{C}$ with the operating temperature of $10 - 12\,^{\circ}\mathrm{C}$ was obtained in this calorimeter. The energy resolution of the calorimeter was obtained at the level of 3−7% [15,16].

The stability of the conversion of the energy released in the crystals into the measured signal should be better than 1% for ensuring high quality of the X-ray images obtained using the MSS. The uniformity and stability of the temperature distribution between the crystals should be within the range of $\pm 0.5\,^{\circ}\mathrm{C}$ for this purpose.

The purpose of the study covered in this article was to create an MSS thermal stabilization system that would ensure long-term uniformity and stability of the crystal temperature distribution of no worse than $\pm 0.5\,^{\circ}\mathrm{C}$ in conditions when the air conditioning system in the room with MSS maintains the temperature in the range of $18-25\,^{\circ}\mathrm{C}$.

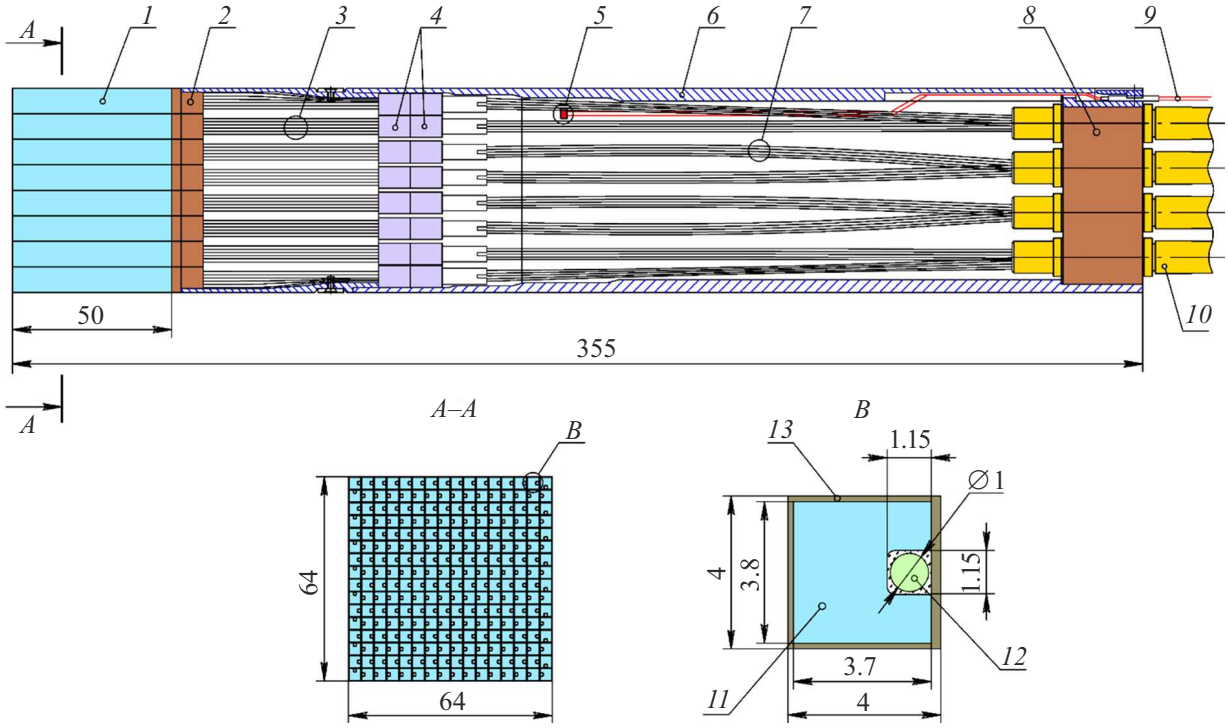

Figure 1. Design of the MSS module. See explanation in the text.

This system has been developed and tested. The liquid cooling cannot be used for thermal stabilization according to the experimental conditions, as in the BGO calorimeter of the detector CMD-3. A fundamentally new solution has been developed for MSS thermal stabilization for this reason. The MSS is housed in a thermally insulated metal case. Photodetectors and electronics are placed outside the enclosure; thus, there is no heat generation inside the enclosure, and the heat flux to the MSS is attributable only to the difference between its temperature and the ambient temperature. MSS uses thermoelectric assemblies based on Peltier elements located on the side walls of the housing for cooling and temperature stabilization.

It was found based on the results of testing of the system that it ensures a long-term stability and temperature homogeneity exceeding the specification level, which made it possible to obtain the maximum energy resolution of a multi-element scintillation screen at the level of 0.5%, which is a record for crystal detectors of this type.

This paper describes the principle of operation of the thermal stabilization system, its component parts and provides the test results.

1. Multi-element scintillation screen

The multi-element scintillation screen is a matrix of 8×8 modules, the front dimensions of the screen are 512×512 mm, length is 355 mm, including 50 mm of the length of crystals. The total mass of BGO crystals is 74.4 kg, the mass of module housings is 70 kg.

Figure 1 shows the design of a separate module.

The recording part *1* of the module is a matrix $A - A$ of 128 recording elements B based on BGO crystals. Each crystal *11* is wrapped in a reflective and light-insulating layer *13*, consisting of 80 μm thick Teflon tape and 20 μm thick aluminum foil. A groove is cut in each crystal along the entire length. A scintillation wavelength shifting fiber *12* is glued into the groove with optical glue, in which the light collected from the crystal is re-emitted for further transmission to the photodetector. Teflon is applied with an overlap to improve the light insulation on the face on which the groove is cut. Thus, two layers of material are obtained on it, which ensures that there are no gaps in the coating and additionally increases the strength of the fiber attachment. The matrix of recording elements is tightly packed externally in an aluminized dacron film with a thickness of 20 μm The wavelength shifting fibers *3* coming out of the crystals pass through connectors *2*. The ends of the fibers are secured in 16-channel optical connectors *4*. Optical cables *10* from photodetectors are connected to the module from the back side. Optical fibers *7* from cables pass through connectors *8* and are connected to the wavelength shifting fibers through optical connectors *4*. Connectors, wavelength shifting fibers, optical connectors and optical fibers are enclosed in a rectangular housing *6* made of duralumin D16T. A temperature sensor *5* is glued to one of the inner walls of the housing, twisted pairs *9* from which are output to the outside behind the housing.

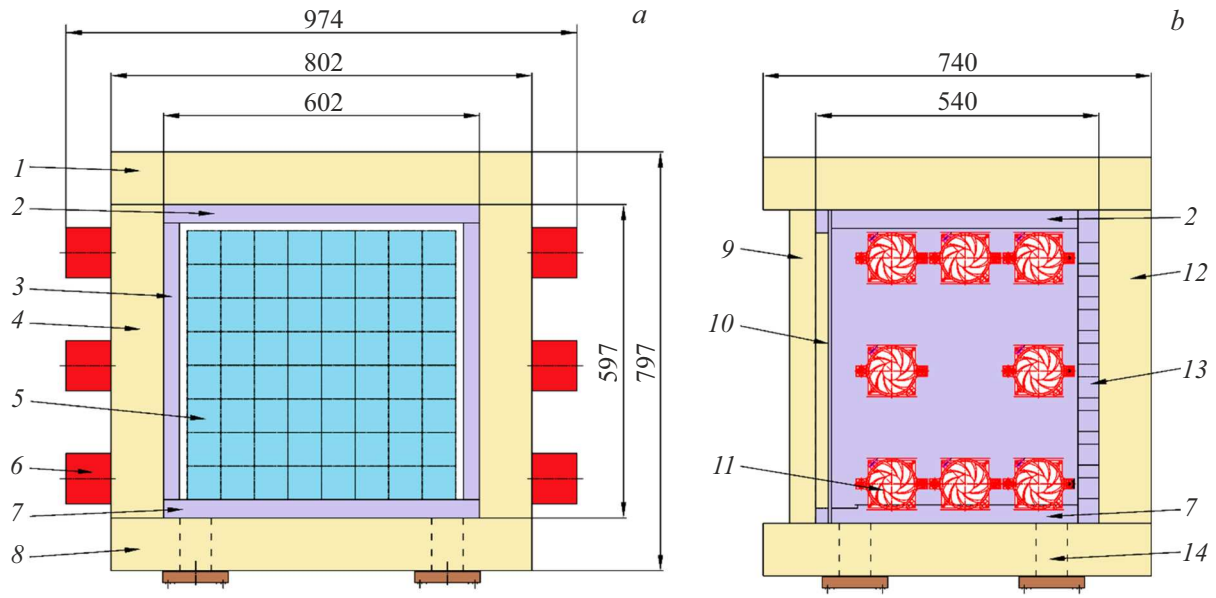

Figure 2. Thermally insulated cooled housing: *a* — front view without front thermal insulation and front screen; *b* — side view without side thermal insulation. *1* — upper thermal insulation; *2* — upper housing cover; *3* — side wall of the housing; *4* — side thermal insulation; *5* — front MSS surface; *6* — thermoelectric assembly duct; *7* — lower housing plate; *8* — lower thermal insulation; *9* — front thermal insulation; *10* — front screen of the housing; *11* — thermoelectric assembly; *12* — rear thermal insulation; *13* — rear wall of the housing; *14* — support.

2. Principle of operation and composition of the thermal stabilization system

The MSS temperature is lowered below the room temperature and maintained at a set level for thermal stabilization. The temperature is lowered in the active mode by the cooling elements, and it is increased in the passive mode by the heat exchange with the environment.

The thermal stabilization system includes:

- thermally insulated housing with cooling elements;
- temperature and relative humidity sensors;
- electronics of the thermal stabilization system;
- software package of the thermal stabilization system.

The MSS is installed inside a thermally insulated housing (Fig. 2), which comprises a rectangular thick-walled metal box covered on all sides with a thermal insulation layer to reduce heat exchange with the environment. The housing is cooled by thermoelectric assemblies based on Peltier elements (Fig. 3) secured on the side metal walls of the housing. The temperature is lowered by supplying power to the thermoelectric assemblies, the temperature is increased by turning off the power. The side walls of the housing are cooled independently by a group of thermoelectric assemblies mounted on the corresponding wall. The main heat exchange between the housing and the MSS is attributable to the contact of the bottom surface of the MSS with the lower plate of the housing, therefore, the readings of temperature sensors installed in the first and last modules of the bottom row of the MSC are used for feedback. are used for feedback.

The temperature is measured using 64 temperature sensors installed inside the housings of the MSS modules, 16 sensors on the side metal walls of the thermally insulated housing installed next to the thermoelectric assemblies, 1 indoor temperature sensor. 4 humidity sensors located inside the thermally insulated housing and 2 indoor humidity sensors are used to measure the relative humidity of the air.

3. Thermally insulated cooled housing

The upper cover, the lower plate, the side and back walls of the metal box are made of aluminum alloy B95, which has a low tendency to deformation after treatment. The thickness of the bottom plate is 35 mm, thickness of side walls is 30 mm, thickness of back wall is 40 mm, thickness of top cover is 35 mm. The weight of the box is 150 kg. The front screen of the box, located between the gamma ray source and the front surface of the MSS, is made of A5M aluminum with a high coefficient of thermal conductivity and has a thickness of 1 mm to minimize the absorption of energy of the recorded gamma rays. The thickness of the front screen was determined based on tests of the thermal stabilization system with the MSS mockup. It was shown that the temperature distribution on the front surface of the mockup does not meet specifications without a front screen, and the use of a screen with a thickness of 1 mm ensures temperature homogeneity with an amplitude of $\pm 0.1\,^{\circ}\mathrm{C}$, the

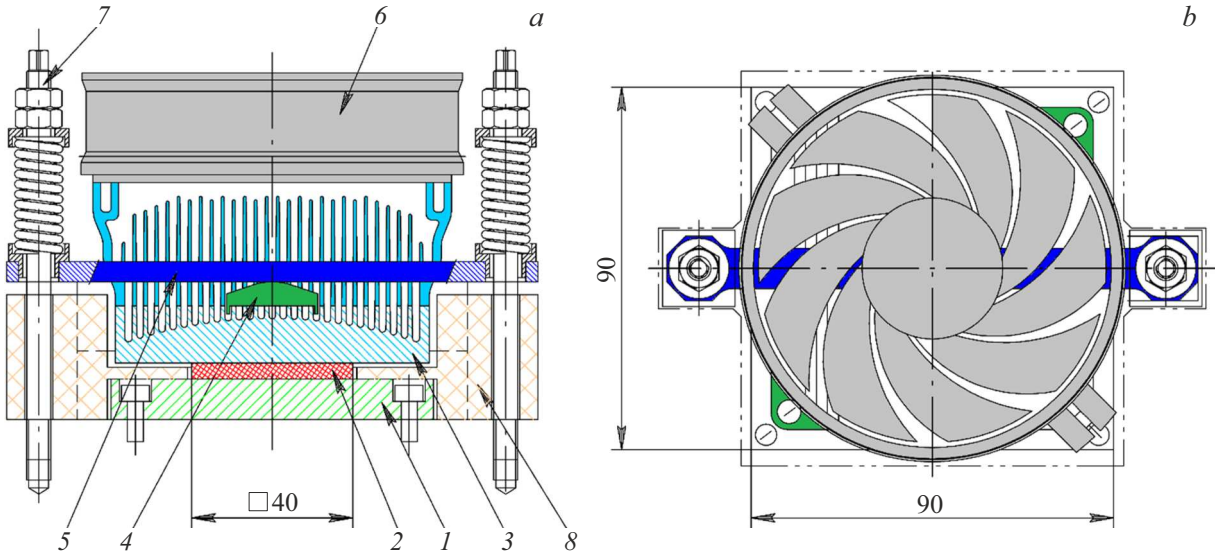

Figure 3. Thermoelectric assembly: *a* — side view, *b* — top view. *1* — copper plate; *2* — Peltier element; *3* — radiator; *4* — spring support; *5* — spring; *6* — fan; *7* — spring-loaded stud; *8* — thermal insulation.

use of a screen with a larger thickness is impractical, since it does not improve the homogeneity.

The bottom plate of the box has four supports made of STEF-1 fiberglass to reduce heat exchange with the support surface on which the housing is mounted.

The metal box was insulated using extruded polystyrene foam with a thermal conductivity coefficient of 0.033 W/(m·°C) and a density of 30 kg/m^3. The thickness of the upper, side, lower and rear thermal insulation is 100 mm. The thickness of the front thermal insulation was reduced to 50 mm to reduce the absorption of gamma-ray energy.

8 thermoelectric assemblies are installed on each of the side walls of the metal box. The thermoelectric assembly consists of a copper plate, which is attached to the wall of the housing with screws, a Peltier element, a radiator and a fan. The radiator and the Peltier element are pressed against the copper plate through a special support by a flat plate spring, the ends of which are secured with spring-loaded studs to adjust the clamping force.

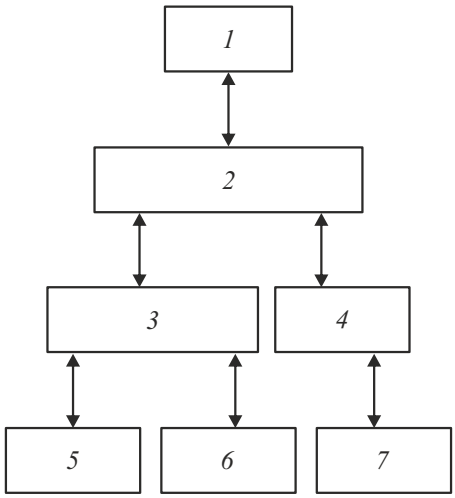

Figure 4. Thermal stabilization system control block diagram: *1* — server, *2* — control electronics, *3* — measuring electronics, *4* — driving electronics, *5* — temperature sensors, *6* — humidity sensors, *7* — thermoelectric assemblies.

4. Electronics of the thermal stabilization system

Thermal stabilization system control diagram is shown in Fig. 4.

The electronics of the thermal stabilization system are divided into three groups: measuring, driving and control. Measuring electronics are designed for interaction with temperature and humidity sensors, driving electronics are designed to control the operating mode of thermoelectric assemblies, control electronics are designed for organizing data exchange. Each of the groups is implemented in the form of independent electronic units based on field-programmable gate arrays (FPGA). This made it possible to increase the maintainability of electronics, increase the upgrading potential, reduce the time for system troubleshooting and repair by replacing blocks.

The operation of the electronics is controlled by a server running the software package of the thermal stabilization system. Information packets are exchanged over an Ethernet network between the server and the control electronics unit.

The control electronics unit includes a single-board microcomputer and a data reception and transmission unit. The control unit interacts with the measuring and driving electronic units according to the commands received from the server using the C-Link interface developed by Budker

Institute of Nuclear Physics of SB RAS, described in Ref. [17], via communication software. It sets the required excitation levels of temperature and humidity sensors for the measuring electronics units, and also receives voltage data from the sensors from them. The power supply data of thermoelectric assemblies are output from the driving electronics units, and the values of the required power levels of Peltier elements and fans determined by the readings of temperature sensors used for feedback are loaded into the driving electronics units.

The driving electronics include eight units. Each unit has two channels for controlling two thermoelectric assemblies. Each channel contains power amplifiers for powering Peltier elements and controlling fan rotation speed.

The functional diagram of the measuring electronics unit is shown in Fig. 5.

The measuring electronics include eleven temperature measurement units and one humidity measurement unit. Each unit contains eight measurement channels. The main nodes of digital signal processing and interfaces of humidity and temperature measurement units are standardized in the FPGA hardware logic. The structure of the input stage and the sensor excitation generator is the essential difference between the units.

Resistance temperature detectors Heraeus M222, type Pt100 are used as temperature sensors: accuracy class 1/3 B (0.1 °C); resistance 100 Ω at a temperature of 0 °C; temperature coefficient of resistance 0.385 Ω/°C; supply current 1 mA. Sensors HIH-4000-003 were used to measure humidity: supply voltage 4.5 V, output signal 0.8−3.8 V, accuracy class 3.5%.

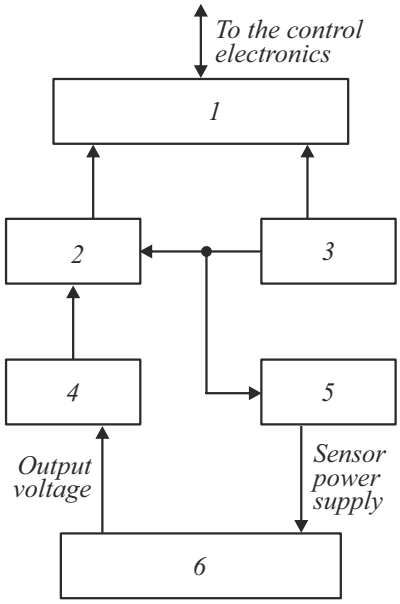

Figure 5. Functional diagram of the measuring electronics unit: *1* — hardware logic, *2* — ADC, *3* — reference voltage source, *4* — barrier filter, *5* — excitation generator, *6* — temperature or humidity sensor.

The potential difference created by the sensors is fed to the input of „barrier filter“ module. This module is used to inhibit interference with an oscillation frequency above 1 kHz. The potential difference from the sensor is then digitized using an 18-bit sequential approximation ADC. Some redundancy in the bit depth of the ADC allows not to use a scaling and shifting preamplifier and, accordingly, resolve the problem of drift of its parameters associated with the temperature, power supply and time, which increases reliability and reduces cost. The ADC operates in the redundant sampling mode, which allows to automatically evaluate the quality of the signal from the sensor, as well as suppress external interference on the cable transmission line of analog sensor signals. The data from the ADC are processed by circuits implemented in the „Hardware Logic“ module.

Fig. 6 shows the wiring diagrams of the sensors.

The reference voltage sources for powering the sensors U_{ref} are based on digital-to-analog converters. The excitation generator of the temperature sensor is based on a precision operational amplifier (OA) and is a stable reference voltage repeater. The output line of the generator is protected from electrostatic discharges by a resistor-diode circuit. The type of OA is chosen so that it is able to withstand an output fault to ground for a prolonged time without causing a board failure. The voltage U_{ref} is maintained at the inverting input due to the negative feedback, the current $I = U_{ref}/R_{lb}$ flows through the sensor under the action of this voltage, and the output signal from the sensor is $U_{sen} = I \cdot R_{sen}$.

The supply currents of the sensors can be slightly different due to the difference of the resistances of the current-setting resistors R_{lb} because each temperature sensor has its own power supply. Each temperature measurement channel is individually calibrated to improve the measurement accuracy. 8 reference resistors with a resistance close to 100 Ω are used for this purpose. The resistance of each resistor is measured with a precision multimeter immediately before calibration using a four-wire connection circuit with an accuracy of 0.005 Ω. The reference resistors are connected after that to eight channels of the temperature measurement unit, and multiple readings are taken, the results of which are averaged. The coefficients of conversion of the measured voltage into the load resistance are calculated based on the measurement results so that this resistance for each channel exactly matches the resistance of the resistor connected to it. These coefficients are entered into the unit calibration database and used later to convert the measured voltage into the sensor temperature. The use of such a technique allows avoiding the need for constant current measurement in each sensor. The accuracy of temperature measurement is ultimately determined by the value of the lowest bit of the measuring ADC, which is 22 μV. The accuracy of temperature measurement associated with the ADC bit rate is limited to 0.057 °C with a supply current of 1 mA since the temperature coefficient of the sensors is 0.385 Ω/°C, and the accuracy is improved by averaging the results

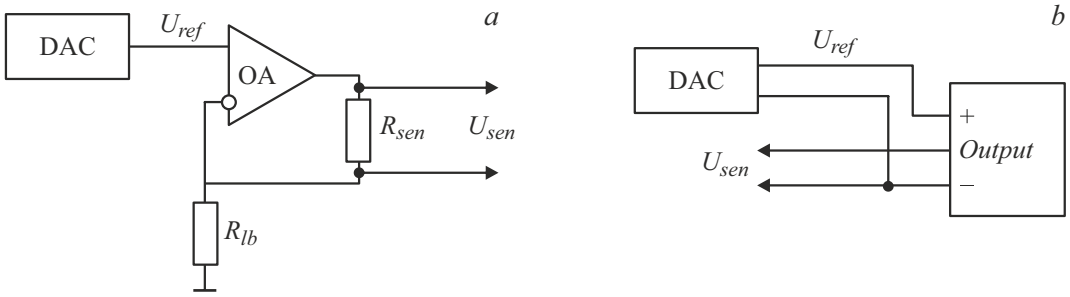

Figure 6. Sensor wiring diagrams: *a* — temperature sensor; *b* — humidity sensor. DAC — digital-to-analog converter, 12 bits; U_{ref} — reference voltage set by DAC; OA — operational amplifier ; R_{lb} — precision current-setting feedback resistor C2-29; R_{sen} — resistance of the temperature sensor; U_{sen} — output measured voltage on the sensor.

of several consecutive measurements. This accuracy is sufficient to measure the temperature heterogeneity of the modules within the permissible limits of $\pm 0.5\,^{\circ}$C.

The temperature and humidity sensors are connected via USB connectors using two twisted pair cables, but the connection circuits differ. The temperature sensors are connected using a four-wire circuit (Fig. 6, *a*): the measuring current flows through one pair of wires, and the voltage is measured on another pair, through which the current practically does not flow. For this reason the parasitic resistance of wires and contacts does not affect the measurement results. Humidity sensors are connected using a three-wire circuit: one twisted pair carries the excitation voltage of the sensor U_{ref}, the other pair carriers the sensor output signal U_{sen}, but the twisted pairs have a common contact at the sensor terminal with a conditional „ground“ (Fig. 6, *b*).

5. Software package of the thermal stabilization system

Structurally, the software is divided into two parts:

1) software operating in the microcomputer of the control electronics unit;

2) software operating in the control server of the thermal stabilization system.

The control electronics unit includes a single-board microcomputer with an installed Linux operating system and a data receiving and transmission unit. The microcomputer has a service program implemented as a server with TCP/IP protocol exchange, receiving commands from control server user programs and sending them to the data receiving and transmission unit via the C-Link interface for further data exchange directly with the driving and measuring electronics units.

The following programs are running on the control server:

- web server that provides a web interface through which the operator controls the thermal stabilization system;
- program for data aquisition from driving and measuring electronics units;
- program for sending data to the PostgreSQL database;
- temperature stabilization program.

A web interface is used to control the thermal stabilization system. The MIDAS software package [18] is used as the basis of the web interface, originally created as a data aquisition system for small and medium-sized experimental physical installations. This software package with additional add-ons is successfully used for Online monitoring and control of the data aquisition system at the CMD-3 elementary particle detector in Budker Institute of Nuclear Physics of SB RAS [19], which was the determining factor for choosing software for the thermal stabilization system. The web interface allows the operator to start and stop the user programs listed above, except for the web server, which is running continuously.

The units provide the program for data aquisition from the driving and measuring electronics units with the values of the voltages on the sensors, the supply voltages of the Peltier elements and fans, as well as the voltages corresponding to the supply currents of the Peltier elements and fans every 60 s. The last 100 values measured in each channel are saved in files and displayed in an Online Database (ODB). The database also stores the temperature, relative humidity and supply current data which are obtained from the measured voltages in accordance with the calibrations stored in the database.

The program every 15 min copies data from files to the PostgreSQL database for long-term storage.

The temperature stabilization program measures the temperature and sets the necessary power levels for Peltier elements and fans, independently from the data aquisition program, depending on the readings of temperature sensors used for feedback.

The operator verifies the measured values using the tables (the last measured values) and graphs, which display the results of the last 100 measurements from the ODB in real time. Information about the operation of the thermal stabilization system in the past can be obtained in the form of graphs from the PostgreSQL database for any period of time specified by the operator.

The MSS and the thermally insulated housing have a significant mass and heat capacity and for this reason their

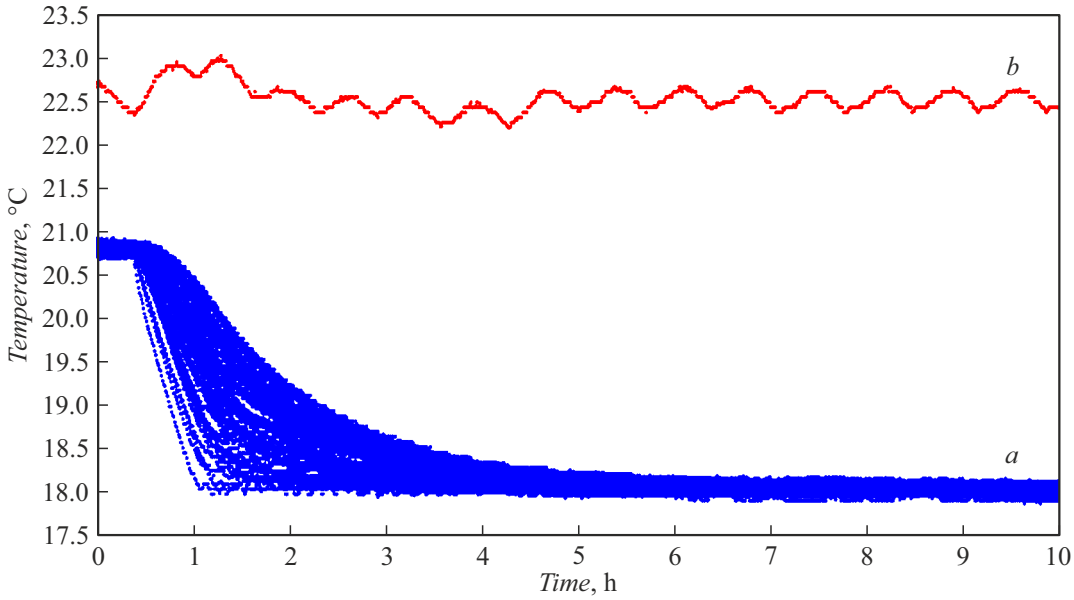

Figure 7. Temperature of the MSS modules (a) and in the room (b) during cooling and temperature stabilization.

cooling and temperature stabilization take a prolonged time. The development includes a scenario in which the thermal stabilization program can be started automatically according to a schedule developed in advance by the operator, without using the web interface.

Unauthorized termination of programs or failures in the operation of electronics can lead to the termination of data exchange and disruption of the thermal stabilization process, therefore, the operator needs tools for timely notification of any interruption in the system. The MIDAS package has a built-in notification system of various levels (warning, alarm), which allows the operator to receive messages about the termination of programs or deviation from the permissible limits of controlled parameters, which may indicate a malfunction of the system. A set of scripts is used to ensure the stability and reliability of the software in addition to the MIDAS built-in control that allows detection of unauthorized termination of programs and automatically restores the programs that should be running at the moment.

6. Thermal stabilization system tests

The commissioning included testing of the thermal stabilization system which allowed to determine the following parameters:

- the time required for cooling of the MSS from the initial temperature to the set temperature level of stabilization and the transition of the MSS to a quasi-stationary temperature condition;
- long-term stability and temperature homogeneity across all MSS modules in stabilization mode;
- the degree of stability of the thermal stabilization regime in any emergency situations, such as the shutdown of part or all thermoelectric assemblies, as well as a rapid short-term change of air temperature in the room where the MSS is placed.

Figure 7 shows a typical cooling schedule for MSS modules. Basically, the modules are cooled due to thermal conductivity through the lower plate of the housing and insignificantly due to contact with the side walls of the housing through its structural elements. As a result, after the start of cooling, the temperature of the modules changes from bottom to top: the bottom row of modules is cooled first, then the other modules are cooled. The temperature difference between the lower and upper modules can reach 3 °C during cooling from the initial state.

The temperature is controlled using the readings of the thermal sensors in the first and last modules of the bottom row. The cooling is continuous with a power close to 12 W per Peltier element as long as the temperature of the lower modules is above the required stabilization temperature.

The stabilization process begins after the temperature of the lower modules reaches the required level: the amplitude of the current supply of the Peltier elements decreases in accordance with the configuration of the thermal stabilization program, and the elements themselves turn on and off so that the temperature of these modules remains constant. The integrated cooling capacity gradually decreases after the stabilization process begins, and the temperature difference between the lower and upper modules decreases. The MSS goes into a quasi-stationary state after some time: the temperature distribution over the MSS field is in a fixed-width corridor for a long time.

Temperature sensors during operation of the MSS cannot be placed directly on the surface of the crystals, therefore they are located on the inner surface of the module housings. Each crystal is wrapped with Teflon tape, which

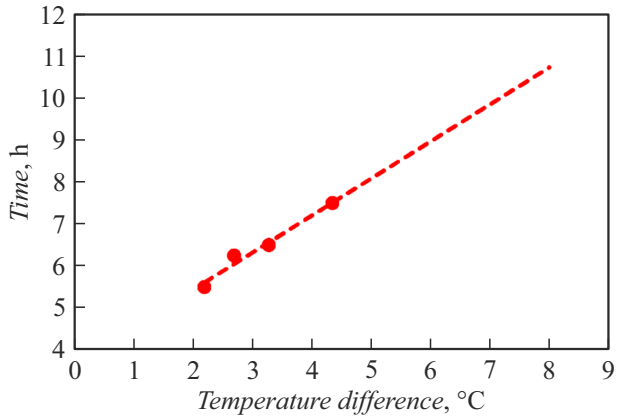

Figure 8. Dependence of the time the MSS module temperature needs to reach the quasi-stationary mode on the difference between the initial and final temperatures.

reduces the transverse thermal conductivity of the crystal matrix and results in a delay of crystal cooling compared to the module housings. 16 additional temperature sensors were installed on the front surface of the crystal matrix to measure the delay time during the tests. The specified delay time of the crystal temperature was 1 h. The results of measurements of the cooling time, stability and homogeneity of the MSS temperature are given taking into account the readings of sensors installed on the front surface.

Figure 8 shows the results of measuring the time interval from the beginning of the MSS cooling to reaching quasi-stationary temperature condition. The measurements were carried out at different initial (19.2–20.8 °C) and final (15–17 °C) temperatures of the MSS, so the result is presented as a time dependence on the difference between the initial and final temperatures. The dashed line shows a linear approximation of the dependence of time on the temperature difference. It is expected that the time to reach the quasi-stationary condition may be 10.7 h with the highest initial temperature of 25 °C and the stabilization temperature of 17 °C.

Figure 9 shows a graph of the temperature of the modules in quasi-stationary condition. The average temperature of the modules is $T_{med} = 17.05\,^{\circ}\mathrm{C}$ with a standard deviation of $\sigma_T = 0.05\,^{\circ}\mathrm{C}$ in long-term quasi-stationary conditions at a given temperature of 17 °C of the extreme modules of the bottom row which is ten times higher than the accuracy of homogeneity and stability of 0.5 °C, defined in the specifications for the thermal stabilization system. The longest period of operation of the system in continuous stabilization mode during the tests was one month.

The resistance of the thermal stabilization system to the impact of emergency situations was tested. The fault tolerance of coolers was studied in the quasi-stationary state of MSS at a temperature of 17 °C, room temperature of 21.8–22.8 °C. The cooler failure was simulated by shutting down half of the thermoelectric assemblies for 2 h. The minimum temperature of the modules remained at a constant level of 16.96–16.98 °C during this period, and the maximum uniformly increased from 17.23 to 17.3 °C.

The resistance to changes of ambient temperature was tested in the quasi-stationary state of MSS at a temperature of 15 °C. The room temperature was 22.4 °C. The room temperature dropped to 16.5 °C during 2 h. At the same time, a decrease of the minimum temperature of the modules by 0.1 °C was observed without further changes until the end of the temperature decrease. Thus, the stabilization mode is resistant to rapid changes of ambient temperature.

The room temperature during MSS warming was 22–23 °C, the initial temperature of MSS was 17–17.3 °C. Fig. 10 shows that the temperature of the modules can remain in the range of 17–18 °C in absolute terms for several hours after the start of warm-up even in case of

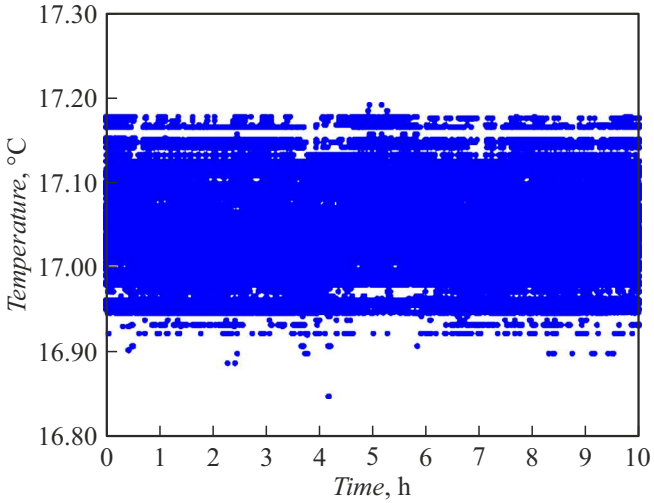

Figure 9. MSS temperature in quasi-stationary thermal stabilization condition.

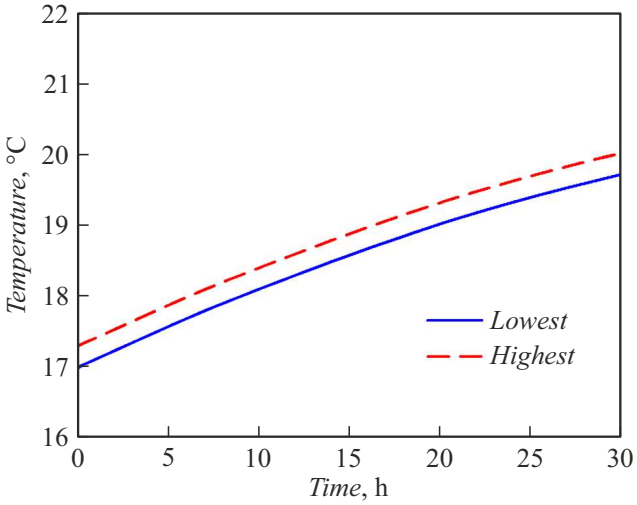

Figure 10. Minimum and maximum temperature of the MSS modules when stabilization is completely disabled.

the complete absence of thermal stabilization, i.e. the homogeneity of temperature distribution across the crystals continues to meet the specifications during this time. Thus, even relatively long interruptions in the operation of the thermal stabilization system cannot affect the quality of the experiment due to the significant inertia of the MSS.

Conclusion

An MSS thermal stabilization system designed for recording hard gamma quantum fluxes has been developed, manufactured and tested. The thermal stabilization system ensures long-term homogeneity and temperature stability of the bismuth orthogermanate crystals used as a material of the screen, while the achieved accuracy of temperature maintenance exceeds the initial specifications by an order of magnitude and equals to $\pm 0.05\,^{\circ}\mathrm{C}$. The system is resistant to various factors, such as the failure of a part of the Peltier cooling elements or a rapid change in ambient temperature. The required homogeneity of temperature distribution $\pm 0.5\,^{\circ}\mathrm{C}$ can be maintained for several hours after the termination of thermal stabilization.

Conflict of interest

The authors declare that they have no conflict of interest.

References

[1] S.S. Afanasenko, R.R. Akhmetshin, D.N. Grigoriev, V.F. Kazanin, V.V. Porosev, A.V. Timofeev, R.I. Shcherbakov. Avtometrija., **57** (2), 82 (2021) (in Russian).

[2] A.V. Timofeev. *Mnogoelementnyj scintillyacionnyj ekran dlya registracii potokov zhestkih gamma-kvantov* (Diss. 2023) (in Russian).
URL: https://www.inp.nsk.su/obrazovanie/dissertatsionnye-sovety#24-1-162-01#faqnoanchor)

[3] C. Cecchi, V. Bocci, S. Germani, P. Lubrano, E. Manoni, A. Rossi, M. Lebeau, M. Bizzarri, G. Chiodi, A. Papi, L. Recchia. J. Phys.: Conf. Series, **293**, 012066 (2011).

[4] D.N. Grigoriev. *Torcevoj kalorimetr detektora CMD-2 na osnove kristallov ortogermanata vismuta* (Diss. IYAF SO RAN, Novosibirsk, 1999) (in Russian).

[5] R.R. Akhmetshin. *Torcevoj elektromagnitnyj kalorimetr na osnove kristallov BGO dlya detektora CMD-3* (Diss. INP SB RAS, Novosibirsk, 2017), URL: http://irbiscorp.spsl.nsc.ru/fulltext/DISSER/2017/Akhmetshin_disser.pdf

[6] F. Kocak. Acta Phys. Polonica A, **131** (3), 527 (2017).

[7] D. Anderson, A. Apresyan, A. Bornheim, J. Duarte, C. Pena, A. Ronzhin, M. Spiropulu, J. Trevor, S. Xie. Nuclear Instruments and Methods in Physics Research Section A, **794**, 7 (2015).

[8] Y. Wei, Yu. Zhang, Zh. Zhang, L. Wu, S. Wen, H. Dai, Ch. Liu, X. Wang, Z. Xu, G. Huang, Ch. Feng, Sh. Liu, Q. An. Nuclear Instruments and Methods in Physics Research Section A, **922**, 177 (2019).

[9] B. Bantes, D. Bayadilov, R. Beck, M. Becker, A. Bella, P. Bielefeldt, J. Bieling, M. Bleckwenn, S. Böse, A. Braghieri, K.-Th. Brinkmann, D. Burdeynyi, F. Curciarello, V. De Leo, R. Di Salvo, H. Dutz, D. Elsner, A. Fantini, O. Freyermuth, S. Friedrich, F. Frommberger, V. Ganenko, D. Geffers, G. Gervino, F. Ghio, G. Giardina, B. Girolami, D. Glazier, S. Goertz, A. Gridnev, E. Gutz, D. Hammann, J. Hannappel, P.-F. Hartmann, W. Hillert, A. Ignatov, R. Jahn, R. Joosten, T.C. Jude, F. Klein, K. Koop, B. Krusche, A. Lapik, P. Levi Sandri, I. Lopatin, G. Mandaglio, P. Mei, F. Messi, R. Messi, V. Metag, D. Moricciani, M. Nanova, V. Nedorezov, D. Novinskiy, P. Pedroni, M. Romaniuk, T. Rostomyan, N. Rudnev, C. Schaerf, G. Scheluchin, H. Schmieden, V. Sumachev, V. Tarakanov, V. Vegna, D. Walther, D. Watts, H.-G. Zaunick, T. Zimmermann. J. Phys.: Conf. Series, **587**, 012042 (2015).

[10] S. Aogaki, F. Takeutchi. IEEE Transactions on Nuclear Sci., **57** (3), 1502 (2010).

[11] C.M. Pepin, Ph. B?rard, A.-L. Perrot, C. P?pin, D. Houde, R. Lecomte, Ch.L. Melcher, H. Dautet. IEEE Transactions on Nuclear Sci., **51** (3), 789 (2004).

[12] H. Zhang, N.T. Vu, Q. Bao, R.W. Silverman, B.N. Berry-Pusey, A. Douraghy, D.A. Williams, F.R. Rannou, D.B. Stout, A.F. Chatziioannou. IEEE Transactions on Nuclear Sci., **57** (3), 1038 (2010).

[13] T.G. Turkington, J.J. Williams, J.W. Wilson, J.G. Colsher, D.L. McDaniel, C.L. Kim, S.G. Ross, C.W. Stearns, S.D. Wollenweber. *Performance of a BGO PET/CT with higher resolution PET detectors.* IEEE Nuclear Science Symposium Conference Record (2005).
DOI: 10.1109/NSSMIC.2005.1596701

[14] NIIC SO RAS: Crystal Growth Laboratory. URL: http://www.niic.nsc.ru/institute/structure/2327-451-crystal-growth

[15] R.R. Akhmetshin, D.N. Grigoriev, V.F. Kazanin, S.M. Tsaregorodtsev, Yu.V. Yudin. Yadernaya fizika, **72** (3), 512 (2009) (in Russian).

[16] R.R. Akhmetshin, D.N. Grigoriev, V.F. Kazanin, A.E. Kuzmenko, Yu. Yudin. J. Instrumentation, **9**, C10002 (2014).

[17] V.M. Aulchenko, D.A. Epifanov, A.N. Kozyrev, I.B. Logashenko, A.S. Popov, A.A. Ruban, A.N. Selivanov, A.A. Talyshev, V.M. Titov, Yu.V. Yudin, L.B. Epstein. Avtometrija., **51** (1), 31 (2015) (in Russian).

[18] S. Ritt, P. Armaudruz, K. Olchanski. *MIDAS (Maximum Integration Data Acquisition System).*
URL: http://midas.triumf.ca

[19] A. Anisenkov, D. Zhadan, I. Logashenko. EPJ Web of Conf., **214**, 01049 (2019). DOI: 10.1051/epjconf/201921401049

Translated by A.Akhtyamov